Resonant-plasmon field enhancement from asymmetrically illuminated conical metallic-probe tips

Ryan M. Roth, Nicolae C. Panoiu, Matthew M. Adams, and Richard M. Osgood, Jr.

Department of Applied Physics and Applied Mathematics, Columbia University, New York, New York 10027

rothr@cumsl.msl.columbia.edu

Catalin C. Neacsu, Markus B. Raschke

Max-Born-Institut für Nichtlineare Optik und Kurzzeitspektroskopie, D-12489 Berlin, Germany

Abstract: Optical-field enhancement and confinement for an asymmetrically illuminated nanoscopic Au tip suspended over a planar Au substrate is investigated both numerically and experimentally. The spatial field distribution of the tip-sample system was calculated using the full 3D finite-difference time-domain method. The calculation enables investigation of the effects of the substrate-tip placement, angle of incidence, and spectral response. The tip plasmon response leads to a significant (up to $\sim$70 times) local field enhancement between the tip and substrate. The enhancement is found to be extremely sensitive to the tip-sample separation distance. Tip-enhanced Raman scattering experiments were performed and the numerical results provide a consistent description of the observed field localization and enhancement.

OCIS codes: (240.6680) Surface Plasmons; (180.5810) Scanning Microscopy; (999.9999) Plasmonics; (999.9999) Field Enhancement.

References and links

1. See, for example, C. L. Haynes and R. P. Van Duyne, "Plasmon-Sampled Surface-Enhanced Raman Excitation Spectroscopy," J. Phys. Chem. B **107**, 7426-7433 (2003).
2. S. Nie and S.-R. Emory, "Probing Single Molecules and Single Nanoparticles by Surface-Enhanced Raman Scattering," Science **275**, 1102-1106 (1997).
3. K. Kneipp, Y. Wang, H. Kneipp, L. T. Perelman, I. Itzkan, R. R. Dasari, and M. S. Feld, "Single-Molecule Detection Using Surface-Enhanced Raman Scattering (SERS)," Phys. Rev. Lett. **78**, 1667-1670 (1997).
4. C. J. Chen and R. M. Osgood, "Direct Observation of the Local-Field-Enhanced Surface Photochemical Reactions," Phys. Rev. Lett. **50**, 1705-1708 (1983).
5. J. L. West and N. J. Halas, "Engineered Nanomaterials for Biophotonics Applications: Improving Sensing, Imaging, and Therapeutics," Ann. Rev. Biomed. Eng. **5**, 285-292 (2003).
6. P. J. Schuck, D. P. Fromm, A. Sundaramurthy, G. S. Kino, and W. E. Moerner, "Improving the Mismatch between Light and Nanoscale Objects with Gold Bowtie Nanoantennas," Phys. Rev. Lett. **94**, 017402 (2005).
7. P. Mühlschlegel, H.-J. Eisler, O. J. F. Martin, B. Hecht, and D. W. Pohl, "Resonant Optical Antennas," Science **308**, 1607-1609 (2005).
8. J.-P. Fillard, *Near Field Optics and Nanoscopy* (World Scientific, 1997).
9. A. Bouhelier, J. Renger, M.-R. Beversluis, and L. Novotny, "Plasmon-coupled tip-enhanced near-field optical microscopy," J. Microscopy **210**, 220-224 (2002).

#67844 - $15.00 USD Received 9 February 2006; revised 27 March 2006; accepted 28 March 2006

10. L. Liu, and S. He, "Design of metal-cladded near-field fiber probes with a dispersive body-of-revolution finite-difference time-domain method," Appl. Opt. **44**, 3429-3437 (2005).
11. T.-W. Lee and S. K. Gray, "Subwavelength light bending by metal slit structures," Opt. Express **13**, 9652-9659 (2005).
12. N.-C. Panoiu and R. M. Osgood, Jr., "Subwavelength Nonlinear Plasmonic Nanowire," Nano Lett. **4**, 2427-2430 (2004).
13. A. Bouhelier, M. Beversluis, A. Hartschuh, and L. Novotny, "Near-field Second-Harmonic Generation Induced by Local Field Enhancement," Phys. Rev. Lett. **90**, 013903 (2003).
14. A. Bouhelier, M. R. Beversluis, and L. Novotny, "Applications of field-enhanced near-field optical microscopy," Ultramicroscopy **100**, 413-419 (2004).
15. C. C. Neacsu, G. A. Steudle, M. B. Raschke, "Plasmonic light scattering from nanoscopic metal tips," Appl. Phys. B **80**, 295-300 (2005).
16. L. Aigouy, F. X. Andreani, A. C. Boccara, J. C. Rivoal, J. A. Porto, R. Carminati, J.-J. Greffet, and R. Megy, "Near-field optical spectroscopy using an incoherent light source," Appl. Phys. Lett. **76**, 397-399 (2000).
17. A. L. Demming, F. Festy, and D. Richards, "Plasmon resonances on metal tips: Understanding tip-enhanced Raman scattering," J. Chem. Phys. **122**, 184716 (2005).
18. C. C. Neacsu, G. A. Reider, and M. B. Raschke, "Second-harmonic generation from nanoscopic metal tips: Symmetry selection rules for single asymmetric nanostructures," Phys. Rev. B **71**, 201402 (2005).
19. A. Hartschuh, E. J. Sanchez, X. S. Xie, and L. Novotny, "High-Resolution Near-Field Raman Microscopy of Single-Walled Carbon Nanotubes," Phys. Rev. Lett. **90**, 095503 (2003).
20. F. Keilmann and R. Hillenbrand, "Near-field microscopy by elastic light scattering from a tip," Phil. Trans. R. Soc. Lond. A **362**, 787-805 (2004).
21. T. Ichimura, N. Hayazawa, M. Hashimoto, Y. Inouye, and S. Kawata, S. "Tip-Enhanced Coherent Anti-Stokes Raman Scattering for Vibrational Nanoimaging," Phys. Rev. Lett. **92**, 220801 (2004).
22. N. Nilius, N. Ernst, and H.-J. Freund, "Tip influence on plasmon exicitations in single gold particles in an STM," Phys. Rev. B **65**, 115421 (2002).
23. J. A. Porto, P. Johansson, S. P. Apell, and T. Lopez-Rios, "Resonance shift effects in apertureless scanning near-field optical microscopy," Phys. Rev. B **67**, 085409 (2003).
24. J. T. Krug, E. J. Sanchez, and S. Xie, "Design of near-field optical probes with optimal field enhancement by finite difference time domain electromagnetic simulation," J. Chem. Phys. **116**, 10895-10901 (2002).
25. W. Denk, and D. W. Pohl, "Near-field optics: Microscopy with nanometer-size fields," J. Vac. Sci. Technol. B **9**, 510-513 (1991).
26. Y. Kawata, C. Xu, and W. Denk, "Feasibility of molecular-resolution fluorescence near-field microscopy using multi-photon absorption and field enhancement near a sharp tip," J. Appl. Phys. **85**, 1294-1301 (1999).
27. A. Downes, D. Salter, and A. Elfick, "Finite Element Simulations of Tip-Enhanced Raman and Fluorescence Spectroscopy," J. Phys. Chem. B (ASAP, 2006), http://pubs.acs.org/cgi-bin/asap.cgi/jpcbfk/asap/pdf/jp060173w.pdf.
28. S. Bruzzone, M. Malvaldi, G. Arrighini, and C. Guidotti, "Theoretical Study of Electromagnetic Scattering by Metal Nanoparticles," J. Phys. Chem. B **109**, 3807-3812 (2005).
29. M. A. Ordal, R. J. Bell, R. W. Alexander, L. L. Long, M. R. Querry, "Optical properties of fourteen metals in the infrared and far infrared: Al, Co, Cu, Au, Fe, Pb, Mo, Ni, Pd, Pt, Ag, Ti, V, and W," Appl. Opt. **24**, 4493-4499 (1985).
30. A. Taflove and S. C. Hagness, *Computational Electrodynamics: The Finite-Difference Time-Domain Method* (Artech House, 2000).
31. U. Kreibig and M. Vollmer, *Optical Properties of Metal Clusters* (Springer, 1995).
32. M. I. Stockman, "Nanofocusing of Optical Energy in Tapered Plasmonic Waveguides," Phys. Rev. Lett. **93**, 137404 (2004).
33. V. Kuzmiak, A. A. Maradudin, "Photonic band structures of one- and two-dimensional periodic systems with metallic components in the presence of dissipation," Phys. Rev. B **55**, 7427-7444 (1997).
34. T. Ito and K. Sakoda, "Photonic bands of metallic systems. II. Features of surface plasmon polaritons," Phys. Rev. B **64**, 045117 (2001).
35. C. F. Bohrena and D. R. Huffman, *Absorption and Scattering of Light by Small Particles* (John Wiley, 1998).
36. Similarly, Malachite Green molecules as adsorbate on planar Au surfaces were studied, as described in detail elsewhere: C. C. Neacsu, J. Dreyer, N. Behr, and M. B. Raschke, (Phys. Rev. B, submitted).
37. M. Moskovits, "Surface-Enhanced Spectroscopy," Rev. Mod. Phys. **57**, 783 (1985).
38. A. D. McFarland, M. A. Young, J. Dieringer, R. P. Van Duyne, "Wavelength-Scanned Surface Enhanced Raman Excitation Spectroscopy," J. Phys. Chem. B **109**, 11279 (2005).
39. K. Karrai, I. Tiemann, "Interfacial shear force microscopy," Phys. Rev. B **68**, 13174 (2000).

#67844 - $15.00 USD Received 9 February 2006; revised 27 March 2006; accepted 28 March 2006

1. Introduction

The optical antenna properties of metallic nanostructures to detect and concentrate light into highly confined regions has attracted considerable interest of late for a broad range of applications. For example, the local optical-field enhancement in colloidal nanoparicles has long been known to be responsible for surface-enhanced Raman scattering (SERS) [1-3] or related photochemical effects [4]. SERS is particularly important in molecular plasmonics for novel analytic and sensor applications [5]. More recently, lithographically produced nanoscale optical antennas of various designs have been demonstrated; this approach allows the plasmonic properties and degree of field enhancement to be tuned [6, 7]. In addition, the field confinement and localization of bare and metal-clad tapered dielectric tips has been demonstrated in scanning near-field optical microscopy (SNOM) [8-10]. Another promising application that has recently been examined is the guiding of light along nano-scale metallic waveguides and nanowires [11, 12].

In contrast, the optical properties of pure metal tips have come under consideration only recently despite their widespread use as probes in atomic-force and scanning-tunneling microscopy (AFM and STM, respectively) [13-18]. Recent applications of metallic-tip optics include scattering-type SNOM (*s*-SNOM) [19-21], photoemission via inelastic tunneling in STM,[22] nonlinear processes such as second-harmonic generation (SHG) driven by local field enhancement [13, 18], and tip-enhanced nonlinear imaging [23, 24]. The signal that can be obtained with these techniques and its spectroscopic signature depend on the strength of the field enhancement located in the tip-sample gap and plasmonic resonances. Both parameters depend sensitively on the exact details of the geometry. This problem has been studied analytically in the *quasi-static* limit, for the special case of a hyperboloid-shaped tip and a field distribution with cylindrical symmetry [25, 26]. However, many experiments (including the one described below) require a more general tip and illumination geometry and analysis in order to understand fully the degree of field enhancement, its material dependance, the exact mechanism of optical tip-sample coupling, and the spectral response of such systems. In addition, other computational methods, such as the multiple multipole method [9] and the finite element method [27] have been used to examine the field structure near metallic tips. However, it is preferable to operate in the time-domain in order to derive the spectral response in one computational run; the computational methods listed above only consider a single frequency at a time.

In this paper, the spatial distribution and spectral characteristics of an optical field generated between a Au nanoprobe and an infinite planar Au substrate, when excited by an incident monochromatic plane wave at an angle to the tip axis, is investigated. A fully-3D finite-difference time-domain (FDTD) method was implemented to calculate the spatial field distribution, spectral characteristics and field enhancement, with the latter defined as the ratio between the local and incident field amplitudes. The numerical results are compared with complementary tip-enhanced Raman scattering experiments using the same geometry. This allows for an experimental test of the calculated enhancement values; in turn the theory provides a consistent interpretation of the microscopic origin of the optical response observed in the experiment.

2. The FDTD model and simulations

The full 3D FDTD numerical method employed to investigate the light interaction with the metallic tip is a particularly effective approach, due to its ability to investigate, without assumptions, arbitrary 3D geometries, including that of the metallic tip, metallic substrate and the illumination geometry discussed here. FDTD also allows the complete spectral response of the system to be calculated in a single computational run, which would not be the case for, for example, the multiple multipole method. The FDTD method also incorporates retardation effects, which can be important for scatterers having dimensions comparable or larger than the

#67844 - $15.00 USD Received 9 February 2006; revised 27 March 2006; accepted 28 March 2006

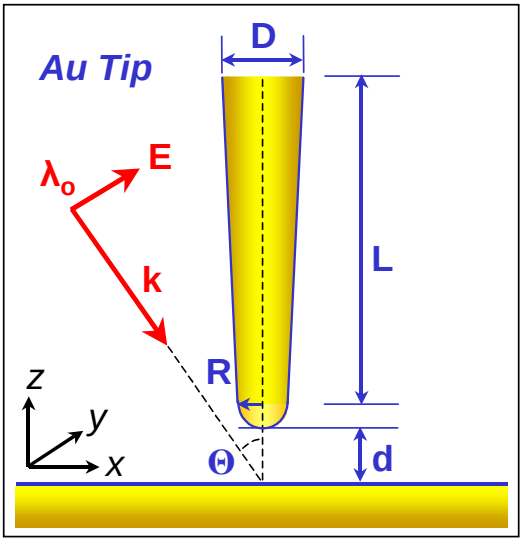

Fig. 1. Schematic of the tip-sample geometry: the Au tip is modeled as a conical taper terminated by a hemisphere of radius R as its point and elevated a distance d above a Au substrate. The tip length, L, and top diameter, D, remain constant for each simulation (800 nm and 200 nm, respectively). An electromagnetic plane wave of wavelength $\lambda_o =$ 633 nm is incident at an angle θ, and is polarized in the $x-z$ plane.

wavelength. Specifically, without including retardation, the effect of induced charges far from the apex cannot correctly be taken into account. Although it was not explored here, the FDTD method can also be used to treat a wide variety of metallic and dielectric materials, rounded and irregular structures [28].

The FDTD algorithm consists of discretizing Maxwell equations on a 3D-grid and then, starting from a given initial condition, marching a set of iterative relations forward in time. Upon choosing a suitably refined computational grid, the corresponding numerical solution gives an accurate representation of the dynamics of the electromagnetic field. Throughout our simulations, we utilized a rectangular computational domain, $L_x \times L_y \times L_z$, of dimensions $400 \times 400 \times 950$ nm^3 surrounded by a 25 nm-thick perfectly matched layer (PML). Both the computational domain and the PML were covered by a $1.41 \times 1.41 \times 1.41$ nm^3 uniform grid. The severe computational requirements of a full 3D FDTD simulation were satisfied using a parallel implementation of the FDTD algorithm, run on a Linux cluster consisting of 18 2.8 GHz Pentium 4 processors. The optical dispersion of Au is accounted for by a Drude dielectric function $\varepsilon(\omega) = \varepsilon_0\left[1 - \frac{\omega_p^2}{\omega(\omega+i\gamma)}\right]$, where ε_0 is the permittivity of free space, and $\omega_p = 13.72 \cdot 10^{15}$ rad/s and $\gamma = 4.05 \cdot 10^{13}$ rad/s the plasma and damping frequencies, respectively [29].

Such a Drude-type dependence of the dispersive optical effects can be rigorously incorporated in the FDTD algorithm [30]. Note that, as is common practice [31], this Drude model, which can be adapted to many materials and excitation wavelength combinations [4], assumes that interband transition effects and dephasing due to electron surface scattering can be neglected. However, the latter can be included by replacing γ with a term dependent on the local-plasmon-system geometry [31]. As we will show later, the frequencies of the resonances exhibited by the tip-substrate system are far from ω_p (i.e., the resonance wavelengths are greater than ~ 200 nm), where these interband transitions are important. Therefore in our simulations we use the Drude model described above.

#67844 - $15.00 USD Received 9 February 2006; revised 27 March 2006; accepted 28 March 2006

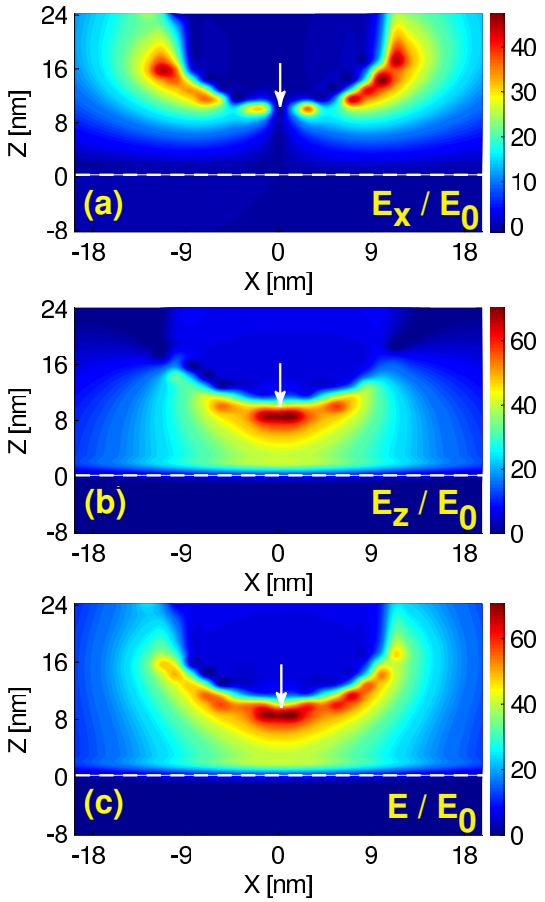

Fig. 2. The $x-z$ section of the time-averaged spatial profile of the steady-state electric field near the apex of the tip normalized to the amplitude of the incident field. The plot shows a) E_x, b) E_z and c) the total field, respectively. For this simulation, $d = 8$ nm, $R = 10$ nm, $\theta = 30^\circ$, and $\lambda_o = 633$ nm were used. The dashed line and arrow indicate the location of the substrate and tip apex, respectively.

#67844 - $15.00 USD Received 9 February 2006; revised 27 March 2006; accepted 28 March 2006

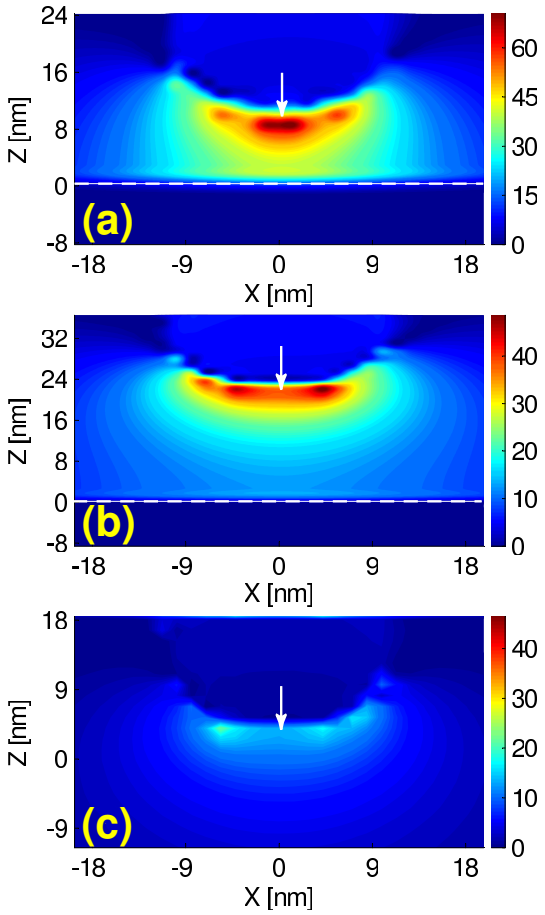

Fig. 3. The field enhancement for E_z for different values of the tip-substrate separation d of (a) $d = 8$ nm, (b) $d = 20$ nm and (c) $d = \infty$ (no substrate). In each case, $R = 10$ nm, $\theta = 30^\circ$, and $\lambda_o = 633$ nm. The dashed line and arrow indicate the location of the substrate and tip apex, respectively.

The geometry of the tip-sample configuration is shown in Fig. 1. The Au tips are modeled as inverted cones, with a base diameter $D = 200$ nm and length $L = 800$ nm. The cone is terminated with a hemisphere having radius $R = 10$ nm. The probe is suspended perpendicularly at a variable distance d above the Au substrate, which defines the $x-y$ plane. The metallic tip is illuminated by a monochromatic plane wave, incident at an angle θ from the z-axis and having a wavelength $\lambda_o = 633$ nm. The incident wave is polarized so that the electric field **E** lies in the $x-z$ plane. The choice of tip length is important, since the field structure of the system may have contributions from both a plasmon propagating along the taper and a localized surface plasmon (LSP) at the apex [32]. However, the computed field structure suggests that the LSP resonance is the dominant source of the field enhancement between the tip and substrate. The tip length, which was limited by our attainable computational domain, was slightly greater than λ_o; this length is known to provide a comprehensive representation of the field structure about the apex [24, 17]. The finite tip length in our computation can effect the locations of the spectral resonances seen in the tip wavelength response. This point is discussed in conjunction with Fig. 5.

#67844 - $15.00 USD Received 9 February 2006; revised 27 March 2006; accepted 28 March 2006

3. Simulation results

The resulting spatial field distribution calculated at $y = 0$ for a $\theta = 30^\circ$ incident light angle and a tip located at $d = 8$ nm above the substrate surface is shown in Fig. 2. Fig. 2(a), 2(b) and 2(c) show the E_x component of the local field (normalized to the incident-field strength E_0), the normalized E_z component, and the total field strength, respectively. These profiles were generated by waiting for the transient computational effects of the CW excitation to dissipate and then averaging the spatial field distributions, which were recorded at 40 time points and equally distributed within a wave period. From Fig. 2, it can be seen that the local field has been enhanced by $\sim 50\times$ for E_x and $\sim 70\times$ for E_z. In every case considered, the E_z component of the field is dominant. This pattern is observed even when θ is small (i.e., small incident E_z). Note that all the fields display a high degree of symmetry about the z-axis, despite the asymmetric illumination. Note also that the finite spatial grid leads to an apparent but artificial roughness of the field at the tip/vacuum boundary; however, as a practical matter the field region of relevance is adjacent to the substrate surface where this roughness is not present.

The results also show that the substrate location has a pronounced influence on the resulting field distribution; this is evident in a comparison of the E_z field profiles at various values of d with $d = 8$ nm, $d = 20$ nm, and $d = \infty$ (equivalent to the absence of the substrate) as shown in Fig. 3(a), 3(b) and 3(c), respectively. The enhancement drops significantly both at the sample surface and the apex surface of the tip as the tip-substrate distance increases.

Figure 4 shows cross-sections of the E_z-field profiles taken at $x = y = 0$ for various d and θ values. In every case, the field peaks in strength near the surface of the tip, and falls off rapidly inside the metal structures, on a length scale set by the skin depth (~ 20 nm for Au). In the lower panel, the dependance of the E_z enhancement on θ is displayed. The effect of tuning θ to maximize the enhancement is much smaller than that achieved by tuning d. The coupling of the incident polarized light beam with the dipole between the tip and substrate apparently results in a relatively insensitive angular dependance of the field enhancement, with an optimum coupling at $\theta = 45^\circ$.

Figure 5 shows the normalized spectral characteristics of the E_z component for various R and d values. To compute these spectra, we used as incoming waves pulses with spectral width $\triangle\lambda = 6\lambda_0$, where $\lambda_0 = 633$ nm. The temporal response of the resulting E_z component near the tip was then recorded and Fourier transformed. The tip response reveals a progression of plasmon-resonance spectral modes. The existence of these peaks in the spectral response has a second practical consequence, namely, that tuning the incident wavelength to one of these peaks in an actual experiment would enhance the system efficiency. Note that a solid metallic cylinder supports a set of plasmon modes whose frequencies converge asymptotically to a frequency limit of $\omega_l = \omega_p/\sqrt{2}$, irrespective of the radius of the cylinder [33, 34]. For Au, the corresponding limiting wavelength is $\lambda_l = 194.3$ nm, which is the same with the asymptotic wavelength to which the resonances in the spectra shown in Fig. 5 converge. It can also be seen that the model accurately predicts no response at short wavelengths (< 194.3 nm). Below this wavelength, the corresponding optical frequencies exceed the plasma frequency of the metal, a range in which the metal behaves as a dielectric; thus there would be no plasmon enhancement.

In addition to the spectral shifts shown in Fig. 5, the plot also illustrates the spectral variation caused by a change in parameters of the tip: d, R, and L. Figure 5(a) shows that increasing d results in a significant blue-shift (~ 50 nm) of the plasmon resonances. These spectral blue-shifts can be attributed to the effective change of the dielectric environment of the scatterer affecting the resonant conditions [35]; similar blue-shifts for tip-substrate systems have been reported elsewhere [17, 23]. Figure 5(b) shows that increasing R acts to reduce the enhancement slightly, with a smaller shift in the spectral response; this trend agrees with the general property of stronger field enhancement near interfaces with smaller radii of curvature. Figure 5(c) illus-

#67844 - $15.00 USD Received 9 February 2006; revised 27 March 2006; accepted 28 March 2006

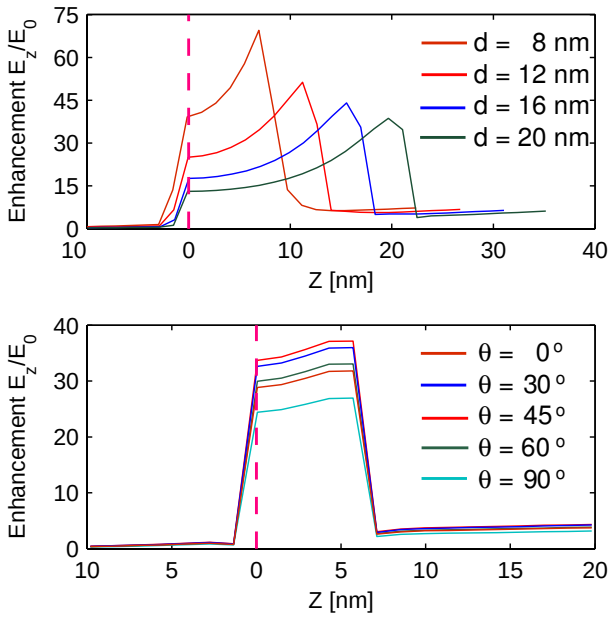

Fig. 4. The enhancement of E_z taken along the $x = y = 0$ line for various values of d and θ. The substrate location is indicated with a dashed line. As expected, the field strength drops off dramatically upon entering the metal tip or substrate and its maximum strength is located just above the surface of the tip. The field enhancement does not vary strongly with incident angle. Here, $R = 10$ nm and $\lambda_o = 633$ nm; $\theta = 30^\circ$ for the upper panel and $d = 4$ nm for the lower panel.

trates the effect of having a finite L for our computation; here, we see that the overall length of the tip, which is limited by the size of the computational domain considered, does play a role in determining the exact positions of the resonance peaks, but that the effect is most pronounced for longer wavelengths which are of lesser interest. The effect at shorter wavelengths is minimal; even smaller (< 200 nm) computational domains have been used [17]. The insensitivity of the shorter wavelength resonances to length and the fact that there is a broad and substantial base to the spectral response makes this plot a useful indicator of the tip wavelength response.

4. Experimental results

In order to provide a direct comparison of the values calculated for the optical field enhancement in the tip-sample gap with experiment, we have performed tip-enhanced Raman scattering measurements. The enhancement can be derived from varying the tip-sample distance for the tip-scattered Raman response. We chose single-walled carbon nanotubes (SWNT) as adsorbate on planar Au surfaces [36]. For the experiment we employ a confocal epi-illumination and -detection geometry, similar to the schematic shown in Fig. 1. Au tips with apex radii r down to $r \sim 10$ nm produced by electrochemical etching [15] were mounted onto a quartz tuning fork of a shear-force AFM [39]. The incoming pump light provided by a HeNe laser ($\lambda = 632.8$ nm) is focused onto the tip-sample gap using a microscope objective (Numerical Aperture $NA = 0.28$, working distance $= 32$ mm, angle of incidence $\theta \simeq 70^\circ$).

For the case when the tip is retracted out of the near-field tip-sample interaction distance the Raman spectrum of SWNT is shown in the inset of Fig. 6. The weak signal observed originates

#67844 - $15.00 USD Received 9 February 2006; revised 27 March 2006; accepted 28 March 2006

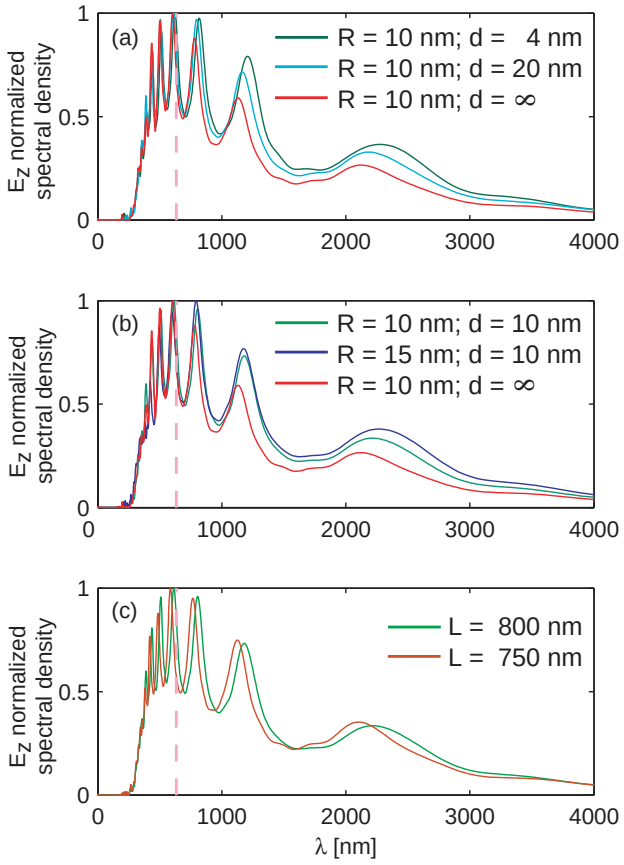

Fig. 5. The spectral response of the tip system for various d (a), R (b), and L (c) values. Various resonant frequencies are present; these resonances can be exploited to make the field enhancement process more efficient. Increasing d can lead to small blue-shifts in the resonant frequencies, while adjusting R only affects the resonant peak amplitude. Note that for $\omega > \omega_p$ (below ~ 200 nm) the actual response deviates due to interband transistions. The dashed line shows the location of $\lambda_o = 633$ nm (~ 1.96 eV). In (c), $R = 10$ nm and $d = 10$ nm.

#67844 - $15.00 USD Received 9 February 2006; revised 27 March 2006; accepted 28 March 2006

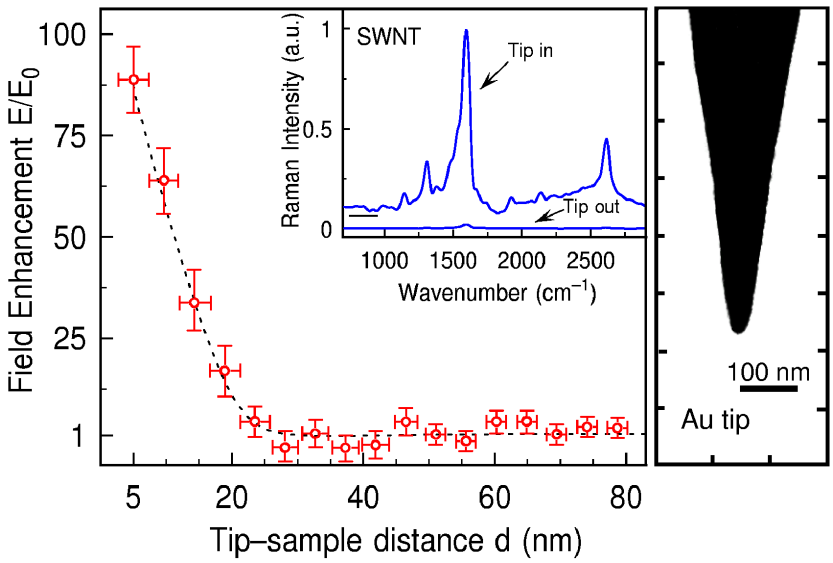

Fig. 6. Optical field enhancement versus tip-sample distance derived from the tip-enhanced Raman scattering experiment (left). Inset: Corresponding Raman spectra for SWNTs on a Au surface with tip at $d \approx 5$ nm ('Tip in') versus tip-sample distance exceeding the near-field interaction length scale ('Tip out'). Right: Electron micrograph of a typical Au tip used for the experiments (scale bar: 100 nm).

from SWNTs within the area of the laser focal spot at the sample surface $A_{\text{out}} \approx 9\ \mu\text{m}^2$. With the tip in force contact with the sample ($d \sim 5$ nm), the observed tip-scattered and -enhanced Raman signal is now emitted predominantly from the near-field confined area of $A_{\text{in}} \sim \pi r^2$ localized around the tip apex in the sample plane. This enhanced near-field region scales with tip radius, as seen from the calculated lateral field distribution shown in Fig. 2(c).

The Raman enhancement factor M for the near-field tip response is then derived as $M \approx I_{\text{in}}A_{\text{out}}/I_{\text{out}}A_{\text{in}}$, with I_{in} and I_{out} being the integrated Raman peak intensities. This results in an enhancement of $M \simeq (1-50) \times 10^7$ for the tip-scattered Raman response with respect to the far-field Raman intensity. The range of values refers to experiments with different tips, since the degree of enhancement varies due to small differences in apex geometry. For both far-field or tip-enhanced processes, the induced Raman polarization is given by $P(\nu_S) = N\alpha_{ba}F(\nu_i)F(\nu_S)E(\nu_i)$. Here N is the number of adsorbates, α_{ba} is the Raman tensor, $E(\nu_i)$ is the incident optical field, $F(\nu_i)$ and $F(\nu_S)$ are the local field enhancement factors for the pump ν_i and Stokes-shifted ν_S frequencies, respectively [37]. Given the comparatively small Stokes shift relative to the plasmon response we assume the fields at the pump and Raman-shifted frequencies to be enhanced equally [38]. With the Raman intensity $I \sim P(\nu_S)^2$, i.e., scaling with the forth power of the field enhancement factor F, the obtained Raman enhancement corresponds to a local enhancement factor of 60 – 150 for the electric field localized in the tip-sample gap. This represents a spatial average across the effective area underneath the tip apex; the exact value of the local enhancement factor is again dependent on the exact apex geometry of the tip used.

The corresponding distance dependence of the local-field enhancement is shown in Fig. 6. As expected the enhancement decays on a length scale of $\sim$ 10nm, i.e., correlated with the tip radius r and in accordance with the theoretical results discussed above. Due to the strong optical near-field coupling between Au-tip and Au substrate, the local field enhancement observed

#67844 - $15.00 USD Received 9 February 2006; revised 27 March 2006; accepted 28 March 2006

exceeds corresponding values derived in previous experiments for SWNTs on glass substrates [19]. The results presented here show a very good qualitative and even quantitative agreement with the theoretical model.

5. Conclusion

This paper reports the results of using a full-3D FDTD method to calculate the field enhancement induced between a metallic tip and metallic substrate by an incident monochromatic wave. The generality of this approach enables an examination of realistic geometries for externally illuminated STM tips. The values of field enhancement calculated for this system are generally more than four times the values reported [17] for similar Au tips suspended over a glass substrate. The increased enhancement provided by the metal substrate indicates that a large range of d values can be used in a given application, whereas the enhancement associated with a dielectric substrate becomes increasingly negligible beyond $d \sim 15$ nm [17]. Thus, any application requiring the highest possible values of enhancement or large tip-substrate separation values would be improved by the use of a metallic substrate. The enhancement factors calculated here were confirmed with tip-enhanced Raman-scattering experiments. Spectrally, the system possesses several resonant peaks above ~ 200 nm, which blue-shift as d is increased.

Acknowledgments

This work was supported by AFOSR contract No. FA9550-05-1-0428. The computer simulation time and cluster work was supported by the Brown University Optocenter (BROWNU-1119-24596). MMA was sponsored by the MRSEC Program of the National Science Foundation under Award Number DMR-0213574 and by the New York State Office of Science, Technology and Academic Research (NYSTAR). CCN and MBR acknowledge support by SFB 658 of the Deutsche Forschungsgemeinschaft.

#67844 - $15.00 USD Received 9 February 2006; revised 27 March 2006; accepted 28 March 2006